Coherent Time Evolution of a Single-Electron Wave Function

M. Kataoka,[1] M. R. Astley,[1,2] A. L. Thorn,[1] D. K. L. Oi,[3] C. H. W. Barnes,[1] C. J. B. Ford,[1] D. Anderson,[1] G. A. C. Jones,[1] I. Farrer,[1] D. A. Ritchie,[1] and M. Pepper[1,2]

[1]*Cavendish Laboratory, J J Thomson Avenue, Cambridge CB3 0HE, United Kingdom*
[2]*Toshiba Research Europe Limited, 208 Cambridge Science Park, Cambridge CB4 0GZ, United Kingdom*
[3]*SUPA, Department of Physics, University of Strathclyde, Glasgow G4 0NG, United Kingdom*

(Received 27 November 2008; published 13 April 2009)

Observation of coherent single-electron dynamics is severely limited by experimental bandwidth. We present a method to overcome this using moving quantum dots defined by surface acoustic waves. Each dot holds a single electron, and travels through a static potential landscape. When the dot passes abruptly between regions of different confinement, the electron is excited into a superposition of states, and oscillates unitarily from side to side. We detect these oscillations by using a weak, repeated measurement of the current across a tunnel barrier, and find close agreement with simulations.

DOI: 10.1103/PhysRevLett.102.156801 PACS numbers: 73.23.Hk, 73.50.Rb, 73.63.Kv

A wide range of modern and future technologies such as quantum electronics, quantum optics, and quantum information processing, rely directly on quantum mechanical dynamics for their operation. For example, the charge state or the spin state of a single electron trapped in a confinement potential, or a quantum dot (QD), is the basis for a quantum-bit (qubit) for various quantum computation schemes [1–8]. Yet the coherent motion of a single-electron wave function is extremely difficult to detect as its time scale is normally in the picosecond regime. Past gate-pulse experiments have successfully investigated the charge states of double QDs containing many electrons [9,10], but never in the single-electron regime where a stronger confinement potential leads to a faster dynamic process, exceeding the experimental bandwidth.

In order to investigate single-electron dynamics here, we take a different approach: moving QDs defined by the potential minima of surface acoustic waves (SAWs) of wavelength $\sim 1\ \mu$m and frequency ~ 2.7 GHz are sent through a static gate-defined circuit [11–13]. These dynamic dots, each containing a single electron, travel past a tunnel barrier at the SAW velocity of ~ 2800 m/s. The potential landscape defined by the surface gates provides a fast-changing time-dependent potential in the rest frame of the dynamic dots. For example, a change in potential over a distance of $0.1\ \mu$m happens in ~ 40 ps. In this way we avoid the bandwidth limitation of experimental circuits without the need for gate pulses.

Eigenstates of a confined quantum system (such as an electron in the ground state of a QD) are stationary in the sense that the probability density of the wave function does not change in time relative to the confinement potential. However, such a quantum state is fragile: a sudden change in the confinement potential can send the electron from the ground state into a linear superposition of eigenstates. The unitary evolution of a single particle in such a superposition of states produces a time-varying probability density. In particular, the probability density arising from a superposition of two eigenstates oscillates with frequency $\Delta E/h$ where ΔE is the energy gap between the two states and h is Planck's constant.

In our dynamic dot, the motion of the electron probability density is induced by the sudden creation of a tunnel barrier in the rest frame of each dot. The fast-changing potential excites the electron into a superposition of states which will oscillate from side to side. Electron tunneling from a QD into a reservoir is usually described by an exponential decay $e^{-t/\tau}$ of the probability of the electron staying in the dot after a time t, where τ^{-1} is the tunnel rate. However, for the case described above, the oscillations of the wave function against the barrier cause an oscillating tunnel rate: the tunnel rate increases when the wave function is close to the barrier because of a larger overlap with a state in the reservoir, but decreases when the wave function is away from the barrier. The transit time past the barrier is fixed by the gate geometry, but the oscillation frequency can be tuned by sweeping gates to change the confinement potential, which leads to an experimentally observable oscillation in the tunnel current, as discussed in more detail below.

This dynamic process can be modeled by numerically solving the single-electron time-dependent Schrödinger equation [14]. The result of this can be seen for a simple time-varying one-dimensional (1D) potential in Fig. 1. Initially, the electron is placed in the ground state of the QD on the left [Fig. 1(a)]. When the barrier potential V_B is suddenly lowered [Fig. 1(b)] the electron is excited into a superposition of states and the wave function oscillates from side to side, periodically hitting the barrier. Figures 1(c) and 1(d) show the time evolution of the probability density of the wave function for the cases of weak tunneling [Fig. 1(c)] and strong tunneling [Fig. 1(d)]. The oscillations are approximately periodic (~ 5 ps period and ~ 0.8 meV excitation gap), because the lowest two states (the ground state $|0\rangle$ and the first excited state $|1\rangle$) are the dominant components (higher states are less likely to be

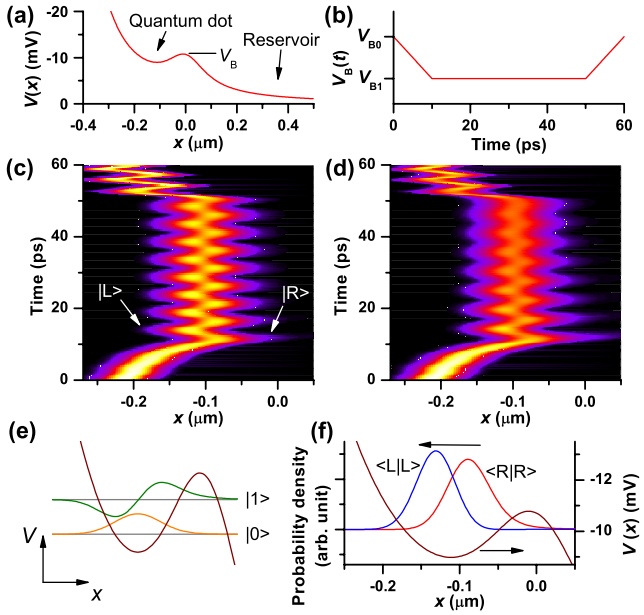

FIG. 1 (color online). Time-dependent one-dimensional model demonstrating the oscillating tunnel rate. (a) Potential across the tunnel barrier is calculated by solving the Laplace equation for the gate geometry of our experimental device. (b) Barrier-gate potential V_B is varied in time. (c) and (d) Time evolution of the probability density of the wave function plotted as a color scale (a brighter color shows a higher value) for the cases of a high tunnel barrier (c) and a low tunnel barrier (d). (e) and (f) Probability density of the two extrema of the wave function $|L\rangle$ (blue) and $|R\rangle$ (red), which can be approximated as a linear combination of the ground state ($|0\rangle$) and the first excited state ($|1\rangle$). The potential profile is plotted in brown.

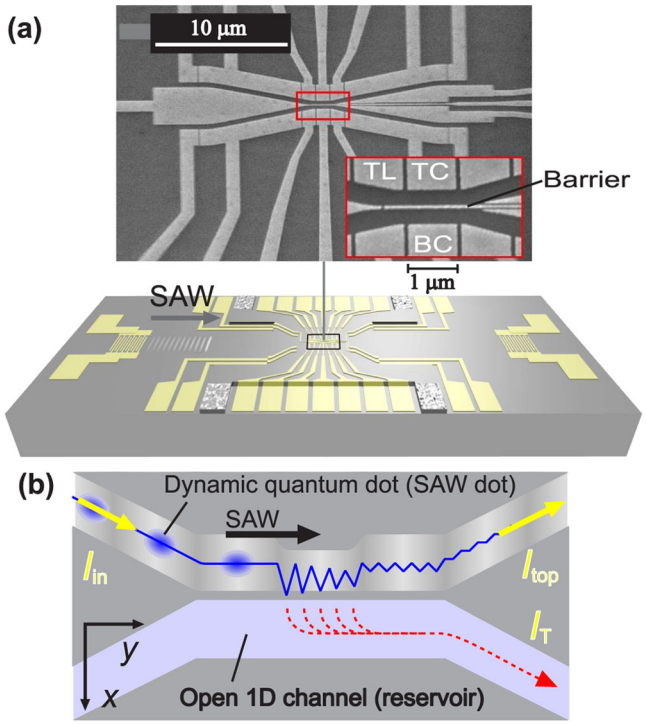

FIG. 2 (color online). Experimental device. (a) Illustration of the sample (bottom) and SEM image showing the surface gates (top). The inset shows the central 3.5 μm $\times$ 2.5 μm of the device. (b) Simplified experimental layout. SAWs carry a single electron in each potential minimum through the completely depleted top channel. At the weakest point of the tunnel barrier, electrons can tunnel into the open 1D channel and escape into the bottom-right exit (dotted line). The solid line in the top channel illustrates the oscillations of the probability density.

excited and escape easily). The wave functions at the left- and right-most positions can be written as $|L\rangle = \alpha|0\rangle - \beta|1\rangle$ and $|R\rangle = \alpha|0\rangle + \beta|1\rangle$, where $|\alpha|^2 + |\beta|^2 \leq 1$, as shown in Figs. 1(e) and 1(f).

In order to investigate these picosecond electron dynamics, we fabricated the device shown in Fig. 2(a) on a GaAs/AlGaAs heterostructure with a two-dimensional electron gas (2DEG) 97 nm below the surface. The 2DEG density was 1.8×10^{15} m^{-2}, and the mobility was 160 m^2/V s. Interdigitated transducers and surface gates were formed by patterning NiCr/Au layers using electron-beam lithography. The transducers were placed 2.5 mm away from the center of the device, where the surface gates define two parallel 1D channels. The transducers and the channels were aligned so that SAWs travel in the [110] direction. Here, only the left transducer in Fig. 2(a) was used. The resonant frequency of the transducer was $f = 2.7149$ GHz. An applied microwave power of 12.8 dBm was pulse modulated with a duty ratio of 1:50 (10 μs pulse length and 500 μs pulse period) in order to minimize sample heating [15]. This also resulted in a reduction of the injected acoustoelectric current to $I_{in} = ef/50 \sim 8.7$ pA (e is the electronic charge) [16].

Prior to measurement, the sample was cooled to 270 mK with a positive bias of 0.3 V on all surface gates [17]. This reduced the effect of switching noise, and the device characteristics were stable throughout the measurements. It also resulted in a shift of pinch-off characteristics by 0.3 V, so that even with zero bias the 2DEG underneath the gates was depleted. The voltages on all 18 surface gates were independently controlled and carefully tuned so that the top channel was depleted, whereas the bottom channel was populated with electrons. The gate voltages were also chosen so that the potential slope along the top channel was shallow enough to keep the electrons confined [18]. Each SAW potential minimum therefore formed a QD [12]. In the bottom channel, from the tunnel-barrier region to the bottom-right 2DEG, an open 1D channel filled with electrons is formed. The effect of the SAW on the bottom channel can be ignored because the SAW potential is screened there [19]. As shown in Fig. 2(a), we label the four gates that define the central region as top left (TL), top center (TC), bottom center (BC), and Barrier.

Each SAW potential minimum captures a single electron from the top-left 2DEG. These electrons are carried through a depleted channel [top channel in Fig. 2(b)],

generating a quantized current I_{in} [11]. As the dynamic QDs pass through the tunnel-barrier region defined by the Barrier, TC, and BC gates, they couple to an open channel [bottom channel in Fig. 2(b)] acting as a reservoir, which is populated with electrons up to the Fermi energy. The entrance region to the bottom channel is strongly pinched off so that SAWs cannot carry electrons into it. Although the lithographic length of the tunnel-barrier region is ~ 1 μm, the actual tunneling region is shorter and is likely to be of the order of ~ 0.1 μm, which gives a tunnel duration of $\tau_d \sim 40$ ps. This arises naturally because the background impurity potential causes a nonuniform barrier height, and the tunneling will be dominated by the weakest point in the barrier.

As illustrated by the solid line in Fig. 2(b), oscillations between the $|L\rangle$ and $|R\rangle$ states are induced when the electron enters the tunnel-barrier region. When the barrier is weak enough, tunneling becomes possible and the wave function decays as shown in Fig. 1(d). The barrier then increases in height again and tunneling is suppressed as the dynamic dots become decoupled from the bottom channel, and the electrons exit into either the top-right or bottom-right 2DEG. The probability that the electron did not tunnel from the dynamic dot is determined by measuring the output current I_{top} from the top channel. In this method, the limitation in τ_d allows us to investigate the dynamics of the electron tunneling without needing to apply short pulses to the electrodes. We also note that, unlike previous charge-coherence experiments where tens of electrons reside in the QDs [9,10], only one electron is trapped in each QD.

Figure 3(a) shows I_{top} as a function of the TC gate voltage V_{TC} while the TL gate voltage is incremented. As V_{TC} is made more negative, I_{top} decreases from the quantized value of the injected current. The reduction in the output current is because the electrons are squeezed towards the barrier, which increases the tunnel current $I_T = I_{\text{in}} - I_{\text{top}}$. At first glance, I_{top} appears featureless (except for a plateau of unknown origin around -0.65 V) showing a smooth change in I_T, as expected from usual electron tunneling behavior. However, removing slowly varying features using a high-pass filter [20] reveals reproducible oscillations with a visibility $\sim 1\%$ of I_{in} [ΔI_{top} in Fig. 3(b)]. Similar oscillations, although with a smaller amplitude and a smaller number of periods, were also observed when the roles of the two channels were swapped.

The behavior of these oscillations is consistent with the theoretical model described earlier (elimination of spurious effects is discussed in Ref. [21]). When V_{TC} is swept, the confinement potential, and hence the excitation gap, changes. If the excitation gap is increased, the frequency of the wave-function oscillation increases. Therefore, the wave function oscillates faster, fitting an extra portion of the oscillations within the fixed tunnel duration. If this extra portion corresponds to the time when the wave function is further from the barrier (mainly in state $|L\rangle$), I_T decreases because the total time for which the electron stays close to the barrier decreases. On the other hand, if the extra portion occurs when the wave function is closer to the barrier (mainly in state $|R\rangle$), extra tunneling will occur and I_T is enhanced [in the experiments, the background in I_T always increases as V_{TC} is made more negative because the tunnel barrier becomes weaker; see Fig. 3(a)]. We note that, although we arbitrarily chose 40 ps as the tunnel duration for this simulation, this should not be taken as a strict requirement for the observation of the oscillations in I_T. We investigated various channel-potential profiles and found that the oscillations in I_T can be observed as long as the number of periods within the tunnel duration is ~ 10 or less. We also note that our tunnel duration is shorter than both the phonon scattering time expected in a QD [22] and the charge-coherence time reported in Ref. [9].

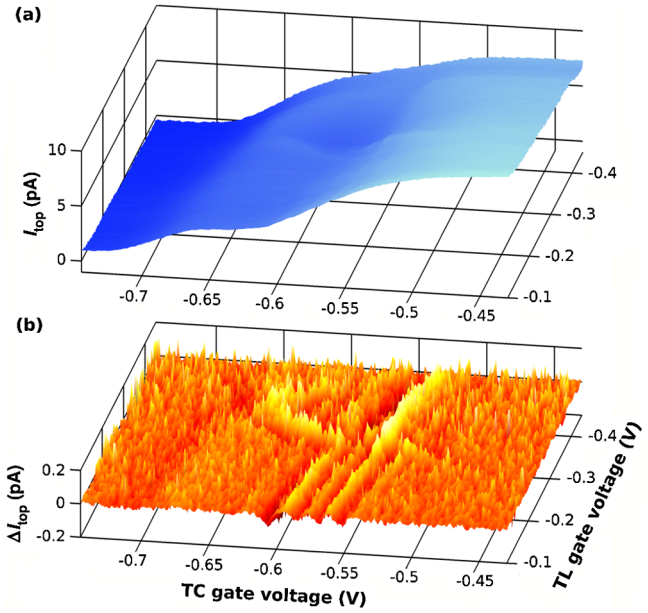

FIG. 3 (color online). The behavior of the output current I_{top} from the top channel as the top- center (TC) and top-left (TL) gate voltages are varied. (a) A plot of I_{top}. As the TC gate is swept negatively, electrons are squeezed out of the top channel, and hence I_{top} decreases from the quantized current $ef/50 = 8.7$ pA. (b) The value ΔI_{top} where slowly varying features are removed by a high-pass filter reveals a set of small-amplitude oscillations. The oscillations gradually die away past -0.3 V. The origin of the crescent-shape feature in this regime is unknown.

In Fig. 4(a) the Barrier-gate dependence of the oscillations in I_T is shown. The oscillations move to a more negative V_{TC} when the Barrier gate is made more negative. This behavior is reproduced using the model described in Fig. 1, where the potential across the barrier is determined by solving the Laplace equation for our gate geometry [23]. Although the actual voltages used are somewhat different (such a discrepancy is expected for this type of potential calculation), similar behavior to the experiments is obtained with comparable periods of oscillation in both

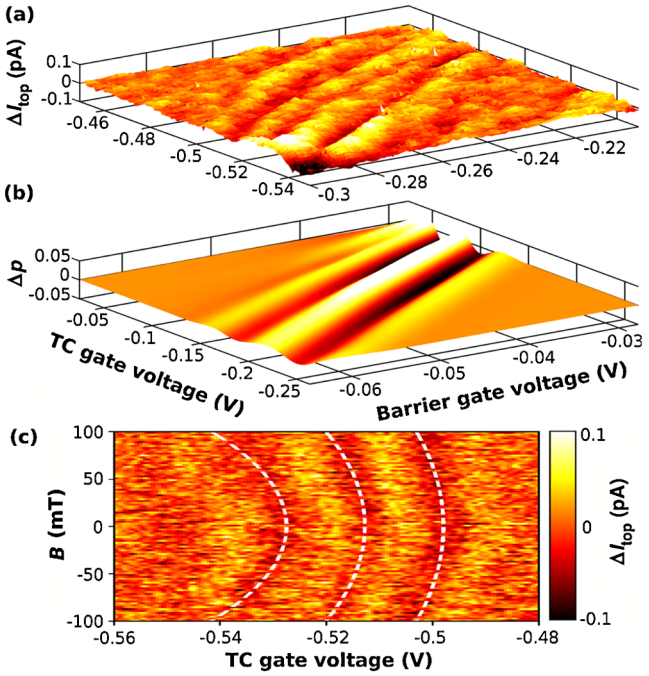

FIG. 4 (color online). (a) and (b) The behavior of ΔI_{top} as the Barrier and TC gate voltages are incremented: (a) Experimental data. (b) Filtered value Δp of the probability p to stay in the dot is plotted from the simulation. (c) Perpendicular magnetic-field dependence. Dotted lines follow the constant excitation gap calculated from a theoretical model of an elliptical QD [24].

gate voltages, as shown in Fig. 4(b). In this regime, making V_{TC} more negative decreases the excitation gap whereas making the Barrier-gate voltage more negative increases the excitation gap. This is consistent with an intuitive picture that, with a weak tunnel barrier, making V_{TC} more negative leads to a larger coupling between the dot and reservoir states and hence to a weaker confinement energy, whereas increasing the barrier potential leads to a stronger confinement.

Further evidence for this model comes from the behavior of the oscillations in a perpendicular magnetic field B [Fig. 4(c)]. The crescent-shaped features correspond to contours of constant oscillation frequency, i.e., constant excitation gap. While a more negative V_{TC} decreases confinement, applying B increases confinement in a QD. The SAW minimum can approximately be considered to be an elliptical dot elongated in the SAW transport direction (in the y direction), because the channel confinement in the x direction is usually much stronger than the confinement by the SAW potential. The oscillation frequency can then be calculated [24] by assuming a SAW amplitude of 20 mV and fitting a linear relationship between V_{TC} and the confinement energy in the x direction. The fit was performed by assuming that the three main dark contours in Fig. 4(c) correspond to N, $N+1$, and $N+2$ oscillation periods. We find good qualitative agreement to the data with $N = 8$, which is consistent with the dynamical simulations in Fig. 1. Our results demonstrate a new technique for the observation of coherent charge dynamics occurring on a few-picosecond time scale. A deeper understanding of such dynamics is important, not only from a fundamental physics perspective, but also in the development of future quantum information technologies such as quantum information processors [1–3].

This research is supported by the UK EPSRC and QIP IRC. We acknowledge the use of computing facilities from CamGrid. M. R. A. thanks Toshiba Research Europe Ltd. for funding. D. K. L. O. thanks the Scottish Universities Physics Alliance.

[1] M. A. Nielsen and I. L. Chuang, *Quantum Computation and Quantum Information* (Cambridge University Press, Cambridge, England, 2000).
[2] D. Loss and D. P. DiVincenzo, Phys. Rev. A **57**, 120 (1998).
[3] C. H. W. Barnes, J. M. Shilton, and A. M. Robinson, Phys. Rev. B **62**, 8410 (2000).
[4] R. Hanson *et al.*, Phys. Rev. Lett. **91**, 196802 (2003).
[5] J. M. Elzerman *et al.*, Nature (London) **430**, 431 (2004).
[6] R. Hanson *et al.*, Phys. Rev. Lett. **94**, 196802 (2005).
[7] J. R. Petta *et al.*, Science **309**, 2180 (2005).
[8] F. H. L. Koppens *et al.*, Nature (London) **442**, 766 (2006).
[9] T. Hayashi *et al.*, Phys. Rev. Lett. **91**, 226804 (2003).
[10] J. Gorman, D. G. Hasko, and D. A. Williams, Phys. Rev. Lett. **95**, 090502 (2005).
[11] J. M. Shilton *et al.*, J. Phys. Condens. Matter **8**, L531 (1996).
[12] M. R. Astley *et al.*, Phys. Rev. Lett. **99**, 156802 (2007).
[13] M. Kataoka *et al.*, Physica (Amsterdam) **34E**, 546 (2006).
[14] W. H. Press *et al.*, *Numerical Recipes in C++: The Art of Scientific Computing* (Cambridge University Press, Cambridge, England, 2002).
[15] R. J. Schneble *et al.*, Appl. Phys. Lett. **89**, 122104 (2006).
[16] M. Kataoka *et al.*, J. Appl. Phys. **100**, 063710 (2006).
[17] M. Pioro-Ladrière *et al.*, Phys. Rev. B **72**, 115331 (2005).
[18] M. Kataoka *et al.*, Phys. Rev. B **74**, 085302 (2006).
[19] J. M. Shilton *et al.*, J. Phys. Condens. Matter **8**, L337 (1996).
[20] A second-order Butterworth filter [P. Horowitz and W. Hill, *The Art of Electronics* (Cambridge University Press, Cambridge, England, 1989)] was applied to the experimental data to create the plots in Fig. 3 and 4, as a function of V_{TC}. A bandpass filter was used for the experimental data to remove the low-frequency background and high-frequency noise. For the results from the simulation, only the low-frequency background was removed.
[21] M. Kataoka *et al.*, Physica (Amsterdam) **40E**, 1017 (2008).
[22] E.g., U. Bockelmann, Phys. Rev. B **50**, 17271 (1994).
[23] J. H. Davies, I. A. Larkin, and E. V. Sukhorukov, J. Appl. Phys. **77**, 4504 (1995).
[24] A. V. Madhav and T. Chakraborty, Phys. Rev. B **49**, 8163 (1994).